PP-Based Nanocomposites with Various Intercalant Types and Intercalant Coverages

Li, Jianming; Ton-That, Minh-Tan; Tsai, Shih-Jung

Publisher's version / Version de l'éditeur:
https://doi.org/10.1002/pen.20552
Polymer Engineering and Science, 46, 8, pp. 1060-1068, 2006-08-01

PP-Based Nanocomposites With Various Intercalant Types and Intercalant Coverages

Jianming Li, Minh-Tan Ton-That
Industrial Materials Institute, National Research Council Canada, Boucherville, Quebec, Canada J4B 6Y4

Shih-Jung Tsai
Union Chemical Laboratories, Industrial Technology Research Institute, Hsinchu, Taiwan 300, ROC

In this article, nanocomposites based on polypropylene containing montmorillonite, modified with two different intercalants (primary and quaternary amine), at three different coverage levels have been investigated. The specimens were prepared in a mini-extruder machine with a counter-rotating configuration. The effectiveness of intercalant type and clay coverage level on the dispersion was analyzed by different means, including X-ray diffraction analysis, field emission gun scanning electron microscopy, transmission electron microscopy, and differential scanning calorimetry. The flexural performance of the specimens was also examined. POLYM. ENG. SCI., 46:1060–1068, 2006. © 2006 Society of Plastics Engineers

INTRODUCTION

Since the pioneering work of Toyota research group on polyamide-6 (PA-6)–clay nanocomposites (NCs) [1], clay-containing polymer NCs, which comprise a polymeric matrix and dispersed nanoclays, have attracted more and more interest from researchers and resin producers because of the significant improvement in physical, chemical, and mechanical performance [2–4]. The improved performance includes higher modulus, superior strength and impact behavior, increased thermal stability, increased solvent resistance, enhanced flame retardancy, and decreased gas permeability when compared to the pristine polymer. Many studies have been focused on polypropylene (PP)-based NCs because of the cost effectiveness of these PNCs in the automotive, packaging, and appliance industries.

Currently, there are three different main approaches to the preparation of PP-based PNCs: the solution process [5–7], in-situ polymerization [8–10], and melt compounding [11–16]. In fact, melt compounding has proved to be an excellent technique because of its ease, versatility, and benign character, with respect to the environment. However, uniform dispersion of nanoclay in the polymer matrix is essential to achieve the improvements mentioned. The nanoclays have a strong tendency to agglomerate because of the natural incompatibility between the hydrophilic nanoparticles and the hydrophobic polyolefin matrix. These aggregates are very difficult to break down by the limited shear force during melt compounding. To break down nanoparticle agglomerates and produce nanostructure composites, many specific approaches have been attempted in recent years. These approaches can be mainly summarized as follows: (i) modification of the clay surface by organo-intercalant [17, 18], or (ii) modification of the polyolefin matrix by incorporating a more hydrophilic compatibilizer [19], or (iii) modification of processing conditions [20–22].

Various efforts have been made to improve the clay dispersion and PNC properties. Ton-That et al. [19] utilized maleic-anhydride-grafted PP (PPMA), with varying molecular weight and acid content, to enhance the interaction with the organoclay. Manias et al. [23] used two approaches, either by using functionalized PP and common organoclay or by using neat PP and a semifluorinated organoclay, to improve the dispersion and the ultimate properties of PP-based NCs. Utracki et al. [24] used an extensional flow mixer combined with twin-screw extruder (TSE) or single screw extruder to improve the dispersion of organoclay in PA- or PP matrix.

However, up to now, full exfoliation of nanoclay in PP by melt compounding has remained difficult to achieve [25–27]; in most cases, the clay in the PP matrix is still in the form of multilayered stacks, with expanded galleries, rather than individual clay platelets. In principle, the PNC formation is thermodynamically driven; therefore, this process can spontaneously happen only with the reduction of free energy during mixing. Consequently, the formation of PNCs is dependent on the interaction between the entropy

Correspondence to: Minh-Tan Ton-That; e-mail: Minh-Tan.Ton-That@cnrc-nrc.gc.ca
Contract grant sponsors: National Research Council Canada; Industrial Technology Research Institute, Taiwan
DOI 10.1002/pen.20552
Published online in Wiley InterScience (www.interscience.wiley.com).

TABLE 1. Material characteristics.

Material (code)	Supplier	Specification
Polypropylene (PP)	Basell Polyolefins	M_w = 250 kg/mol
Polybond 3200 (PPMA)	Crompton	M_w = 84 kg/mol, MA wt% = 2.0
Cloisite Na	Southern Clay Products	Pristine montmorillonite
Cloisite 15A (Q120)	Southern Clay Products	Montmorillonite intercalated by dimethyl di(hydrogenated tallow) ammonium chloride with a clay surface coverage of ~120%
Cloisite 20A (Q100)	Southern Clay Products	Montmorillonite intercalated by dimethyl di(hydrogenated tallow) ammonium chloride with a clay surface coverage of ~100%
Modified clay (Q60)	IMI self prepared	Montmorillonite intercalated by dimethyl di(hydrogenated tallow) ammonium chloride with a clay surface coverage of ~60%
Modified clay (P120)	IMI self prepared	Montmorillonite intercalated by excess octadecyl amine of ~20%
Modified clay (P100)	IMI self prepared	Montmorillonite intercalated by octadecyl amine with clay surface coverage of ~100%
Modified clay (P60)	IMI self prepared	Montmorillonite intercalated by octadecyl amine with clay surface coverage of ~60%

and enthalpy factors. Obviously, the conformational entropy of the polymer chains decreases when they are forced to be confined inside the organoclay interlayer.

To balance the penalty originating from the polymer chains confinement, it is crucial to form an initial organoclay structure, to be able to significantly increase its dispersion in the polymer matrix, thus increasing the entropy of the system. This could be achieved by a larger initial gallery gap resulting from the intercalant with longer aliphatic tails and high intercalant coverage on the clay surface. However, high intercalant coverage is not always better, because the reactive sites on the clay surface could be hindered. Therefore, intercalants should not be too crowded on the clay surface if there is good interaction between the compatibilizer and the clay. Kim et al. [28] presented self-consistent field simulation results for a PNC that is composed of four components; clay, short chain intercalant, long chain end functionalized compatibilizer, and host polymer were considered in the model. They concluded that, to achieve exfoliation, the surface of the organoclay should be partially bare for interacting with a compatibilizer. In addition, it is important that the clay must chemically react with the compatibilizer. Compared with quaternary amine, a primary amine intercalant that contains active hydrogen would be expected to provide greater reactivity with the maleic anhydride group of the compatibilizer. However, this issue has not been fully considered so far. For PP-based NCs, a compatibilizer is always required. Moreover, the molecular weight of the compatibilizer should be considered to ensure that no phase separation takes place with respect to the host polymer.

Accordingly, the objective of this study is to investigate the influence of the type of intercalant and the coverage level on the clay surface of the dispersion, the PNC structure (morphology and crystallinity), and mechanical properties. More specifically, the organoclays have been treated with primary amine (octadecyl amine) and quaternary amine (diethyl di(hydrogenated tallow) amine), intercalant with three different surface coverage levels of 60, 100, and 120%.

EXPERIMENTAL PROCEDURES

Materials

A series of PNC samples were prepared from the same PP matrix and compatibilizer, and the same formulation with various organoclays. The source and the characteristics of the raw materials are listed in Table 1.

Treatment of Clays

The treatment of clays was done according to methods described elsewhere in the literature [27]. The molar ratio between the intercalant and the clay ion exchange capacity, i.e., the "surface coverage," was 60, 100, and 120%. The primary-amine-treated clay was designated as P, while the quaternary amine one was Q. The Q120 and Q100 samples were based on Cloisite 15A and Cloisite 20A, respectively (Table 1).

Preparation of PNCs

Compounding. Prior to melt compounding, the PP, PPMA, and all the organoclays were dried under vacuum at 90°C for 24 h. Melt compounding was carried out using a mini-extruder machine with a counter-rotating configuration. The compounding strategy involved two steps: (i) master-batch preparation, followed by (ii) dispersive dilution with the addition of PP. In the stage of master-batch preparation, PPMA and organoclay, in the ratio of 4:1, were dry-blended and fed into the mini-extruder machine. Compounding was carried out under a blanket of dry N_2 at a screw speed of N = 100 rpm, mixing temperature T = 190°C, and mixing time t = 5 min, using a circulation mode. After that, the master-batch material was diluted by the addition of PP to obtain a final content of organoclay in the PNC of 2 wt%, using the same parameters as in master-batch preparation. Details of the formulation can be seen in Table 2.

Injection Molding

The ultimate specimens were injection-molded using a mini-injection-molding machine, with a chamber temperature of 200°C and a mold temperature of 100°C. The specimens were 35 mm long, 12 mm wide, and 1.2 mm thick.

Analysis and Characterization

X-ray Diffraction. The X-ray diffraction (XRD) measurements were performed on a Bruker D8 Discover, with Cu Kα radiation. XRD scans were obtained using an incident X-ray wavelength of $\lambda = 0.15406$ nm, at a scan rate of 1.5°/min. The specimens were mounted horizontally in the holder. The spectra were obtained using slits of 0.1, 0.6, and 1 mm, sweeping the 2θ range from 0.8 to 10°.

Field Emission Gun Scanning Electron Microscopy. The samples were prepared by cutting a rectangular plate in the middle, polishing the surface, and then removing the amorphous domains by chemical etching, to improve the contrast between the clay and the matrix. The observation was made on a field emission gun scanning electron microscopy (FEGSEM; HITACHI S-4700), with the working operation voltage of 2 kV.

Transmission Electron Microscopy. The samples were microtomed under liquid nitrogen ambient with a diamond knife, using a Leica Ultracut FC microtome. The nominal thickness of the section was 70 nm. The section was transferred from water to 200-mesh Cu grids. A transmission electron microscope (TEM), JEOL JEM 2011, at an acceleration voltage of 200 kV was used for direct observation of organoclay dispersion in the PNC.

Differential Scanning Calorimetry. Crystallization behavior was studied using a Perkin Elmer Pyris-1 series differential scanning calorimetry (DSC). Samples were heated from 30 to 200°C at a rate of 20°C/min, and then cooled from 200 to 30°C at the rate of 10°C/min under nitrogen atmosphere. The heat of fusion was determined by integrating the DSC exotherm. The crystallinity was determined as the ratio of the latent heat of fusion of the sample with respect to the theoretical latent heat of fusion of 209 J/g, for 100% crystalline PP.

TABLE 2. Description of the PP, PP-PPMA, and PNCs.

Designation	Loading and organoclay type	Loading and compatibilizer type
PP		
PP-PPMA		8 wt% of Polybond 3200
NPQ120	2 wt% of Q120	8 wt% of Polybond 3200
NPQ100	2 wt% of Q100	8 wt% of Polybond 3200
NPQ60	2 wt% of Q60	8 wt% of Polybond 3200
NPP120	2 wt% of P120	8 wt% of Polybond 3200
NPP100	2 wt% of P100	8 wt% of Polybond 3200
NPP60	2 wt% of P60	8 wt% of Polybond 3200

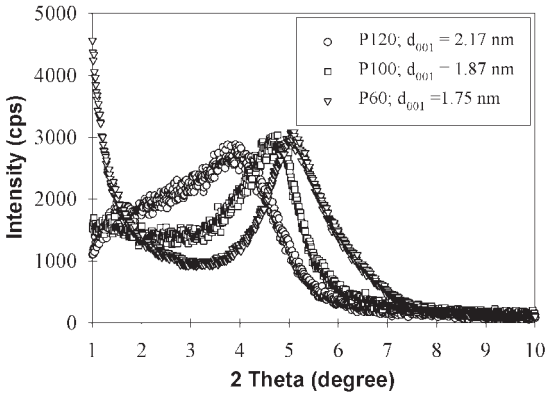

(a)

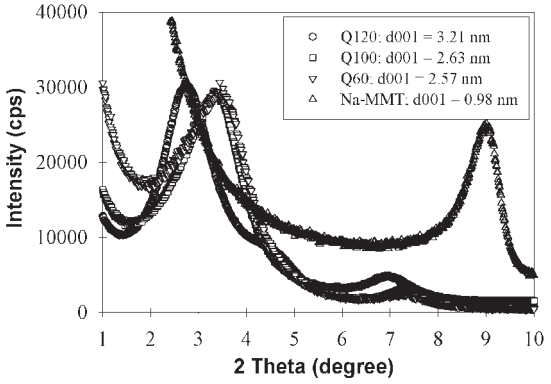

(b)

FIG. 1. XRD patterns of pristine organoclay containing (a) primary amine intercalant and (b) quaternary amine intercalant and pristine montmorillonite.

Flexural Testing. Flexural behavior was tested on an INSTRON 1125 machine with a cell of 500 kg, at a crosshead speed of 5 mm/min, at room temperature (23°C). The property values reported here represent an average of five tests.

RESULTS AND DISCUSSION

Dispersion

The spectra of Na-montmorillonite clay (Na-MMT) and the treated clays are illustrated in Fig. 1a and 1b. Na-MMT gives the lowest d_{001} value of 0.98 nm. The d_{001} values of the organoclays are greater than that of Na-MMT, indicating good intercalation of the clay by the intercalants. In general, quaternary amine intercalants (Fig. 1b) provide higher d_{001} values than their primary amine counterparts (Fig. 1a). This can be easily understood in terms of the greater steric effect of the quaternary amine, which consists of two long hydrocarbon chains (hydrogenated tallow), while the primary one composes only one. It is also noticed that the higher the clay surface coverage, the greater the gallery distance. This is simply a result of the greater amount of intercalant in the

 DOI 10.1002/pen

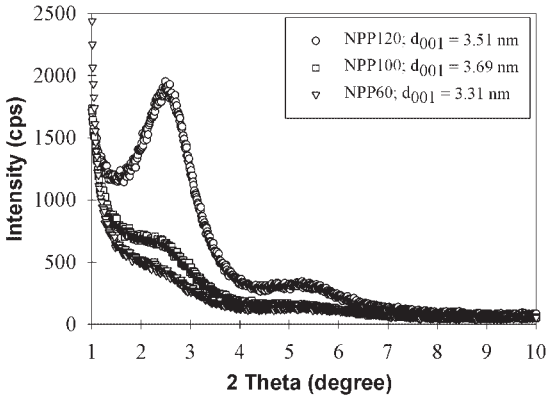

FIG. 2. XRD patterns of NPP120, NPP100, and NPP60. The composition of PNC is 90 wt% PP:8 wt% PPMA:2 wt% organoclay.

system. Sample Q120 displays the largest d_{001} value that is 3.21 nm.

Figure 2 presents the XRD spectra of NPP120, NPP100, and NPP60. Compared with the XRD spectra of pristine organoclay, the XRD spectra of the PNCs shift to lower angles, indicating that the organoclays have been further intercalated by either the compatibilizer or the PP or both. It should be stressed here that the increase of d_{001} is more meaningful than the gallery distance, because it represents the quantity of compatibilizer or polymer that has entered the galleries, which describes the level of interaction between the matrix and the clay. The increase of d_{001} value in the PNCs is quite significant, namely 1.34 nm for NPP120, 1.82 nm for NPP 100, and 1.56 nm for NPP60. For NPP100 and NPP60, such an increase is due to the penetration of compatibilizer or PP into the clay gallery, while for NPP120 it can also be due to the replacement of the excess intercalant (which is not chemically bonded on the clay) by a compatibilizer or matrix. Obviously, the largest interlayer spacing was observed in the NPP100 system (100% clay surface coverage), whose gallery distance (3.69 nm) remains almost the same as that of the NPP120 (3.51 nm). So far, the results indicate that the level of the intercalant coverage has a certain effect on the intercalation of organoclay in the PP matrix, but the d_{001} values of these three samples are comparable. This may imply that the clay interlayer expansion depends mainly on the compatibility between the polymer and the organic intercalant or clay attribute or both and the chemical interaction between the two phases. Nevertheless, the intensity of the XRD peak does decrease with the reduction of intercalant coverage. Reduction of the X-ray peak intensity can be caused by different factors, but the two more important ones for this case should be either the reduction of the intercalated clay aggregates due to exfoliation or the compaction of the clays to form large aggregates. To verify the cause of the peak intensity reduction, SEM and TEM observations were conducted.

FEGSEM is a very useful tool for observing clay dispersion and PNC microstructure. Figure 3 shows the FEGSEM photos for the PNC-containing clay, with a primary amine intercalant. Obviously, NPP120 has a very fine dispersion, although there can be seen a very few, but large aggregates (Fig. 3a). Large and medium and small aggregates were observed in NPP100 (Fig. 3b), but the large and medium ones are smaller and more numerous than in NPP120. For NPP60, the number of medium and large aggregates increases, although the size of the large aggregates decreases (Fig. 3c). It should be noted here that big aggregates can be found in all cases, but it cannot be shown for all samples here. At first glance, this phenomenon seems to be rather odd. From the simulation [28], one might expect that the

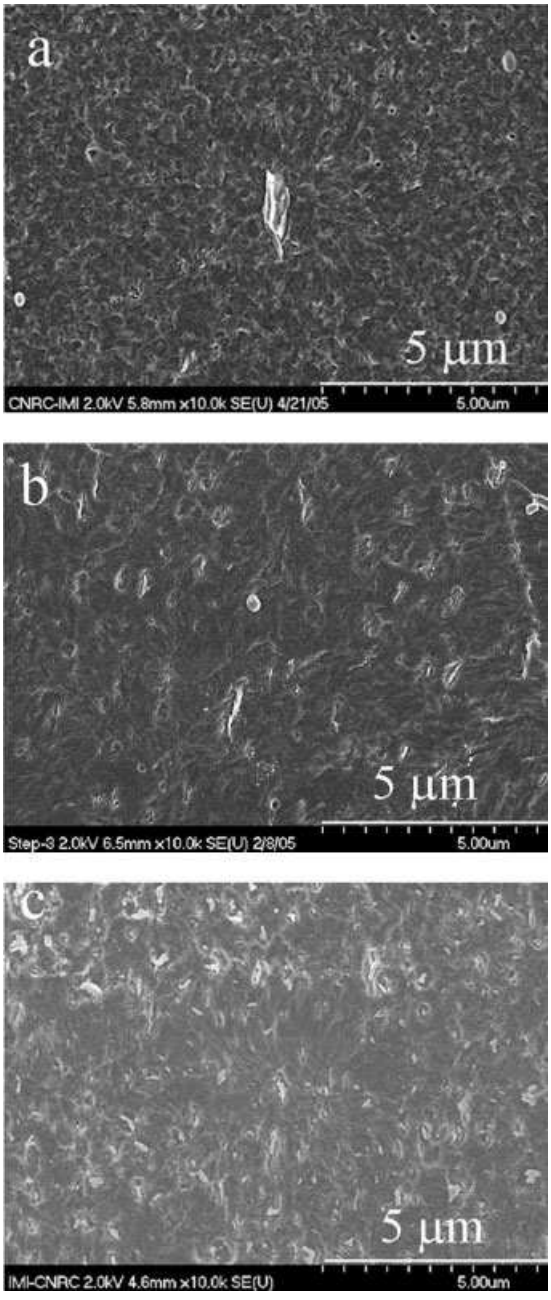

FIG. 3. FEGSEM photomicrographs for (a) NPP120, (b) NPP100, and (c) NPP60.

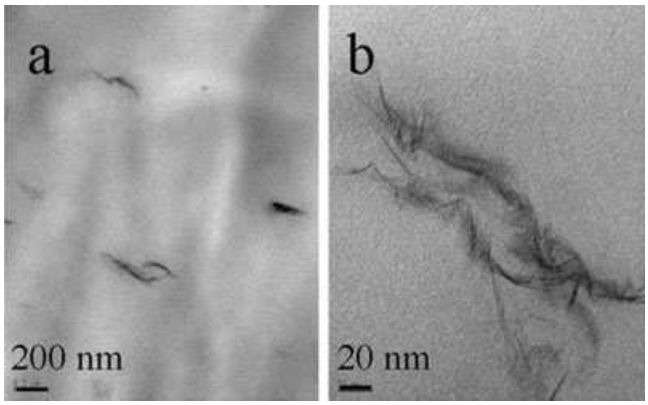

FIG. 4. TEM photomicrographs for NPP120; (a) in low magnification and (b) in high magnification.

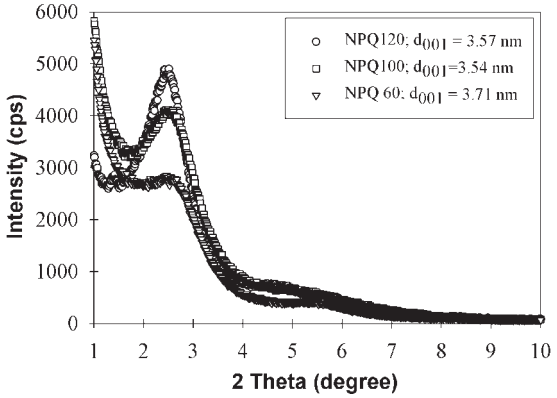

FIG. 6. XRD patterns of NPQ120, NPQ100, and NPQ60. The composition of PNC is 90 wt% PP:8 wt% PPMA:2 wt% organoclay.

dispersion should get better on going from NPP120 to NPP60, because there will be a higher possibility for interaction between the compatibilizer and the bare clay surface. However, the experimental results show quite the opposite. There are several different explanations that can be considered. First, the initial gallery distance of the NPP60 is smallest, which means greater clay–clay interaction. As a result, it is more difficult for the compatibilizer to overcome this interaction in order to enter the clay gallery. Second, the bare clay surface has high hydrophilicity that reduces the compatibility with the PP matrix. Third, if thermal degradation of intercalant takes place to some extent, the clays in the NPP60 can be blocked more easily than the others.

The TEM photos in Figs. 4 and 5 reveal the structures for NPP120 and NPP60, respectively. The dark and bright regions correspond to the clay and PP matrix, respectively. The low magnification image clearly shows the existence of clay clusters in NPP120, indicating a poor clay dispersion (Fig. 4a). However, it is interesting to observe that at high magnification (Fig. 4b) the cluster shows a loose and disordered structure. Poor dispersion was also seen for NPP60, as shown in Fig. 5a. However, in contrast with NPP120, at high magnification (Fig. 5b), these clusters possess a well-aligned densely compacted structure. This reconfirms the XRD and SEM results for the poor clay intercalation and dispersion of this sample. No sign of partial exfoliation can be observed, and so the reduction in the peak intensity of the NPP60 is more likely due to agglomeration.

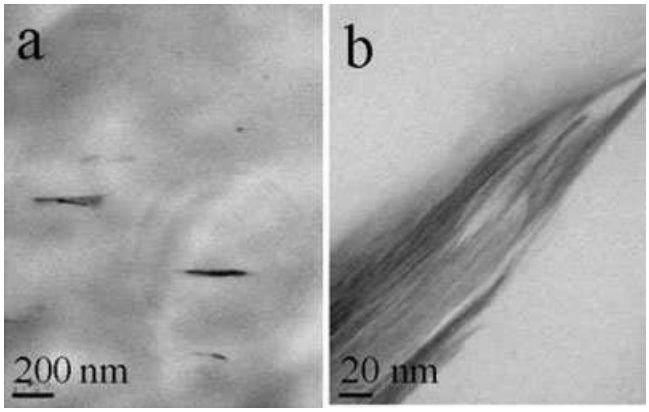

FIG. 5. TEM photomicrographs for NPP60; (a) in low magnification and (b) in high magnification.

Figure 6 gives the XRD spectra of NPQ120, NPQ100, and NPQ60. An increase in d_{001} was observed for all three samples as a result of further intercalation of compatibilizer/PP matrix in the clay galleries. Although the d_{001} values of the three samples are more or less the same and also comparable to that of the NPP series, there is a large difference in the increase of d_{001} between them. Among the NPQ series, NPQ60 has the highest value of 1.14 nm. This can be explained by the fact that bare clay surface can provide a better chance for the allocation of compatibilizer in the clay gallery, while the high intercalant coverage levels of Q120 and Q100 somehow limit the intercalation of compatibilizer/PP. However, this observation is different for the NPP series, possibly because the initial gallery distance of the P clay series is much smaller, which causes much more difficulties for the entrance of the compatibilizer/polymer for the NPP60. It can also be observed from Fig. 6 that the XRD peak intensity of NPQ does decrease with the reduction of intercalant coverage level. As discussed earlier, the reduction of peak intensity can be due to clay agglomeration.

Figure 7 presents the FEGSEM photos for NPQ120, NPQ100, and NPQ60. Figure 7a shows a very fine dispersion of clay for NPQ120, with very few but large aggregates. The image of NPQ100 is very similar to that of NPP100, although the size of the small aggregates is slightly greater. However, for NPQ60 (Fig. 7c), two populations of clay dispersion are clearly observed, mainly composed of fine stacks, with a significant amount of large aggregates. The presence of the partially bare clay surface can provide a better intercalation as discussed earlier, but its drawback is a poorer microdispersion. The presence of a larger amount of large aggregates in NPQ60 can be due to the nonhomogeneous intercalation of the pristine clays, since the amount

 DOI 10.1002/pen

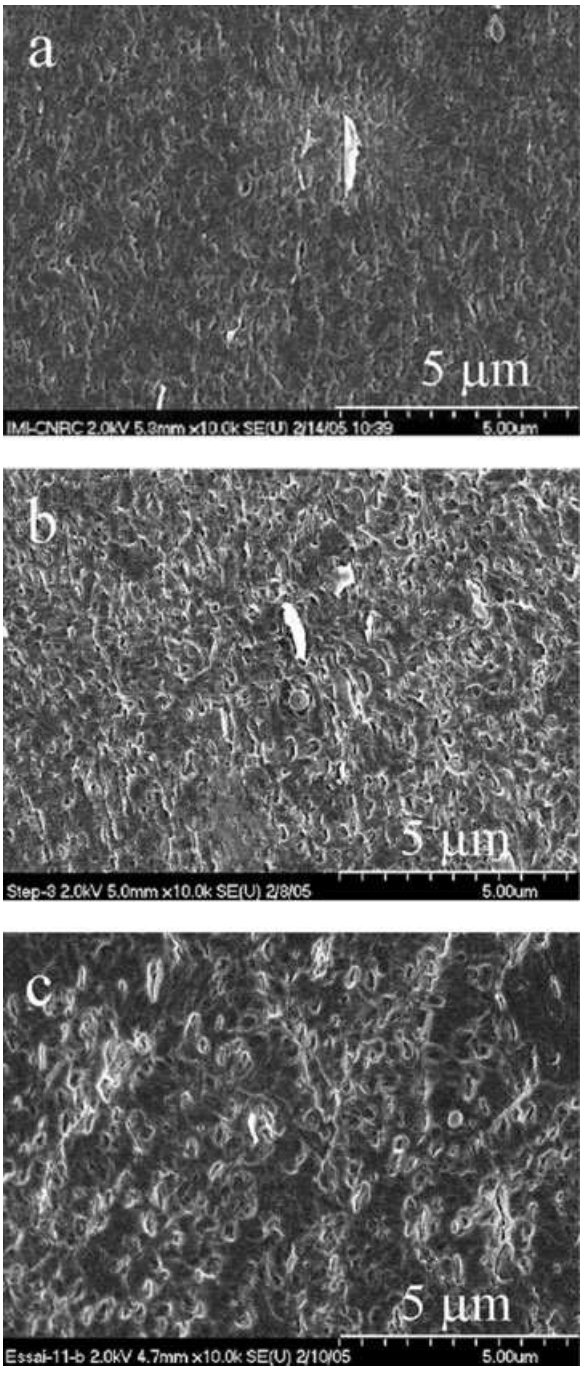

FIG. 7. FEGSEM photomicrographs of (a) NPQ120, (b) NPQ100, and (c) NPQ60.

of the intercalant is too small as compared to the others, or to some other reason.

Figures 8 and 9 show the TEM micrographs of NPQ120 and NPQ60, respectively. Both intercalated and exfoliated structure can be found in these samples, but NPQ120 provides better and more uniform nanodispersion. As seen in Fig. 8a, besides the fine stacks, including single, double, triple, and multiple platelets, the presence of a few big stacks can also be observed. On further amplifying the image of the large stack (Fig. 8b), a compacted and well-ordered layer structure was found. The interlayer spacing in this stack is about 1.8 nm, which is far from the d_{001} value obtained from XRD. This explains the heterogeneity of clay intercalation by the onium ion. Whatever the origin, this layered structure with limited gallery distance is very difficult to break into small stacks because of the strong clay–clay interaction. Figure 9 shows the TEM micrograph for NPQ60. Multilayer stacks with partially exfoliated structure were observed (Fig. 9a and 9b). On focusing on the aggregate and amplifying, it is very interesting to observe a very loose layer structure (Fig. 9b), which is quite different from the well-ordered layer structure of the stack in NPQ120 (Fig. 8b). It is expected that this loose structure can be readily converted to an exfoliate structure, under intensive processing conditions or the use of a higher amount of compatibilizer. The destruction of the ordered structure of the clay in NPQ60 should be the result of a good interaction between the bare clay surface and the compatibilizer. This loose structure also explains why the size of the aggregates in NPQ60 significantly increases, as seen in Fig. 7c. In other words, the observation of large aggregates by SEM does not always mean that the clays have a poor dispersion in the matrix. It should be stressed here that, to have a better understanding of the dispersion of nanoclays, one must

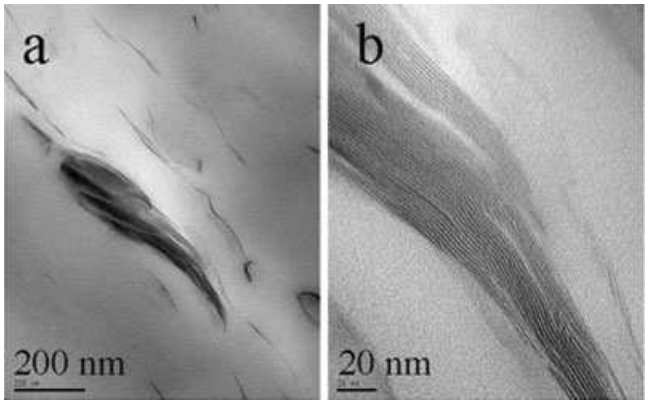

FIG. 8. TEM photomicrographs of NPQ120; (a) in low magnification and (b) in high magnification.

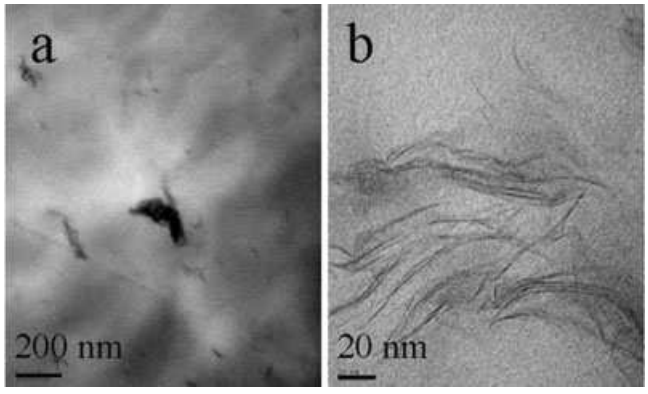

FIG. 9. TEM photomicrographs of NPQ60; (a) in low magnification and (b) in high magnification.

carefully look at the particles at different levels and angles. Reviewing the XRD patterns for the NPQ series, the decrease in peak intensity with the reduction of intercalant coverage level could be attributed to the loose (disordered) structure of the clay layers in the stacks.

Even in the poor shear conditions of the mixing device, significant differences in the structure of PNCs can be observed. Overall, the NPQ series exhibits a better nanodispersion, which comprises intercalation and exfoliation, while only an intercalated structure can be observed for the NPP series. This can be explained by the difference in the initial gallery distance. The P clay series has a much smaller gallery distance than the Q series. As a result, it is much more difficult to break down the aggregate to form a fine dispersion. In the NPP series, the nanodispersion becomes worse with the reduction of intercalant coverage level. However, in the NPQ series, the aggregate structures changed in the reverse way, that is, from a well-aligned compact layered structure to a loose and disordered one. The main issue here is also the difference of the gallery distance of the starting clays. In both cases, the use of excess intercalant P120 and Q120 can provide better intercalation, but the greater gallery distance of the starting clay Q120 compared to P120 is an advantage in terms of improving the microdispersion and giving a more uniform distribution. Also, the P60 and Q60 provide a greater increase in clay gallery distance on going from clay to nanocomposite, but the drawback is poorer microdispersion with less uniformity. The same experiment conducted in high shear mixing device (TSE) has confirmed an improvement of dispersion and uniformity. The results of the work will be presented in the next publication.

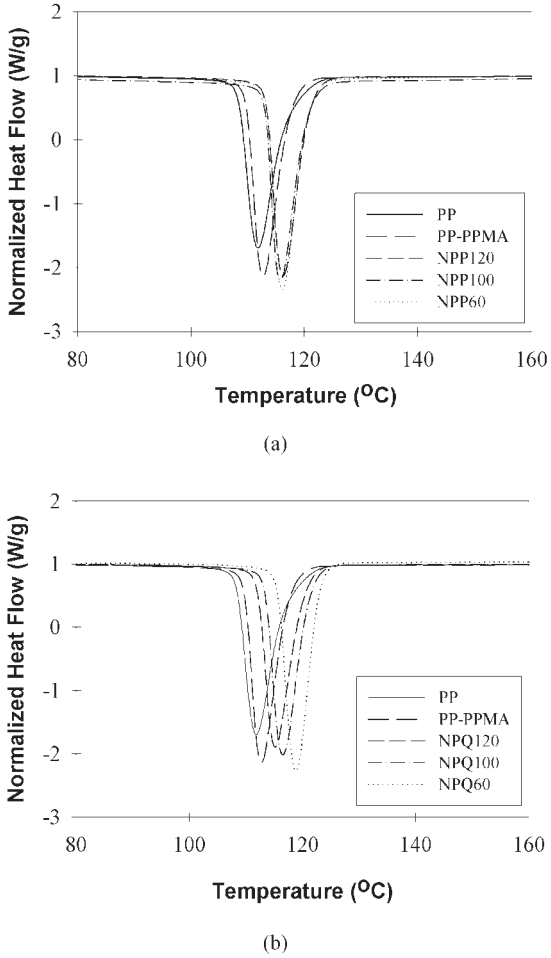

FIG. 10. DSC thermograms of (a) PP, PPMA, NPP60, NPP100, and NPP120; (b) NPQ60, NPQ100, and NPQ120. (Cooling scans at the rate of 10°C/min).

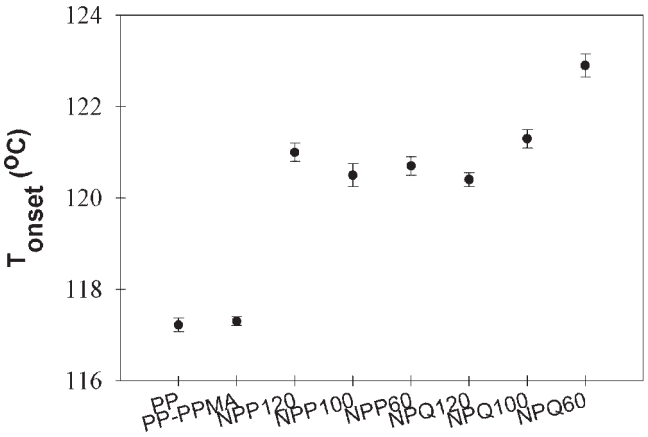

FIG. 11. T_{onset} for PP, PP-MA, and PNCs.

Crystallinity

DSC measurements of PP, PP-PPMA, and PNCs were carried out to determine the effect of intercalant type and intercalant coverage on the crystallization behavior of NC. Figure 10 shows exothermic peaks, representing the crystallization of the pristine PP, PP-PPMA, and PNCs. From Fig. 10, it is obvious that PP and PP-PPMA are quite identical in terms of the starting crystallization temperature (T_{onset}) and the exothermic peak position, while those of the PNCs shift to higher temperature (Fig. 10). For a better comparison, Fig. 11 shows the T_{onset} for the PP, PP-PPMA, and PNCs. The identical T_{onset} for PP and PP-PPMA indicates that the addition of compatibilizer does not affect the crystallization of PP. However, the addition of P-type organoclay to the PP/compatibilizer matrix shifts T_{onset} from 117.2°C for PP to 121°C for NPP120, 120.6°C for NPP100, and 120.7°C for NPP60. Earlier crystallization (i.e., higher T_{onset}) was also observed for their Q-type counterparts in the NPQ series, but appeared to increase significantly with the reduction of intercalant coverage levels. This raises the question of why the difference of T_{onset} is so marginal for the NPP series and so detectable for the NPQ series. For the P-type clay, the active primary amine intercalant would be expected to readily interact with the compatibilizer and reduce the nucleation effect, while for the Q-type clay, the quaternary amine, which has two long hydrocarbon chains, would be expected to show more affinity with the PP matrix, resulting in a finer dispersion. However, surprisingly, the

 DOI 10.1002/pen

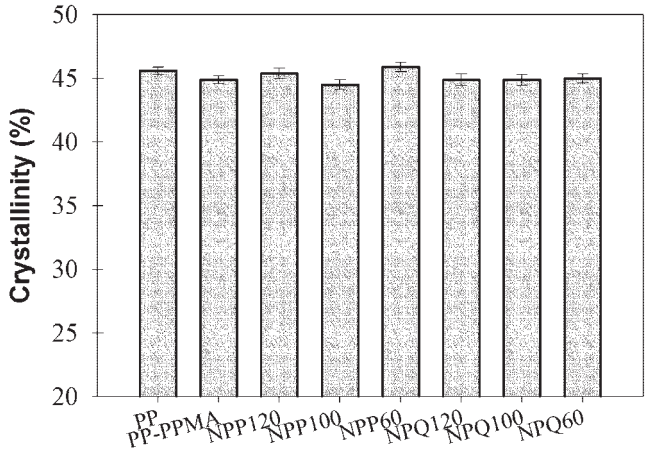

FIG. 12. Crystallinity for the PP, PP-PPMA, and PNC, respectively.

study of the crystallinity of PP, PP-PPMA, and PNCs, shown in Fig. 12, does not give any significant indication of the effect of intercalant and intercalant coverage levels. Why does the addition of nanoclay accelerate the crystallization process, but not increase the crystallinity? Probably, on the one hand, the partial exfoliation of organoclay increases the nucleation effect and accelerates the crystallization process, while on the other hand, in PNCs, the confined PP segment in the organoclay interlayer will be restricted, resulting in a decrease in the number of crystalline PP chains. In addition, the absorption of the PP or compatibilizer molecules on the clay surface may also affect the crystallization behavior of NC. Nevertheless, this issue still remains to be understood.

Flexural Performance

To evaluate the effect of intercalant type and coverage on the mechanical performance of the resulting PNCs, flexural testing was done on the PNC specimens. Figure 13 presents the flexural strength and flexural modulus for the PP, PP-PPMA, and PNC specimens. It is clear that the addition of PPMA to the matrix PP has no significant impact on the flexural behavior. As expected, the addition of 2 wt% of organoclay significantly improves both the strength and modulus in all cases. From the results obtained earlier, it seems that the NPQ series has a better performance than does the NPP series. This can be explained by the finer and more uniform dispersion of clay in the NPQ series. It was also expected that the NPP series could provide a higher rupture stress, since the primary amine intercalant can provide a better chance for chemical interaction between the clay and the matrix via the active hydrogen of the primary amine. However, such expectations are not confirmed. The intercalant coverage level of the organoclay showed no effect on the flexural behavior of the NPP series, but it does for the NPQ series. The flexural properties of NPQ120 and NPQ100 are quite similar, but the flexural performance of NPQ60 is lower. Although the TEM observations demonstrated that NPQ60 has better intercalation and more interaction between the clay and the matrix, based on the loose structure of the aggregates (Fig. 9). The FEGSEM micrograph indicates poor dispersion for this sample. In other words, the microstructure (microdispersion) has played a more important role in determining the flexural properties of this sample.

CONCLUSIONS

PP/PPMA/organoclay PNCs, with various intercalants and intercalant coverage levels, were prepared to investigate the effect of intercalant type and intercalant coverage level on the dispersion and mechanical performance. As evidenced by XRD, all the clays, though involving different intercalant type and coverage level, were well intercalated in the PP matrix. Aggregates with various extents were observed in all of the PNC specimens by FEGSEM, indicating strong clay–clay interaction during melt compounding. For the NPP series, TEM revealed that with the reduction of intercalant coverage the clay aggregates changed from a loose and less-ordered structure to a well-aligned and densely compacted layered structure during melt compounding, while the opposite phenomenon was observed for the NPQ series. The addition of organoclay to the PP/compatibilizer matrix increases the onset crystallization temperature, but not the crystallinity. Intercalant coverage level also showed detectable effects on the T_{onset} for the NPQ series, but not for the NPP series. No significant effect of intercalant type and coverage level on the crystallinity of PNC was recorded. The flexural performance of the NPQ series, in general, is better than that of its NPP counterpart. Reducing the intercalant coverage resulted in a decrease in flexural performance of NPQ. However, the flexural performance of the NPP series appeared to be independent of intercalant coverage level. For obtaining NCs with better dispersion/performance, it is necessary to increase the gallery distance of the clay (probably not smaller than 20 Å) prior to melt compounding, to favor the penetration of comapatibilizer and PP molecules into the interlayer of the clay during melt mixing. Furthermore, an intensive com-

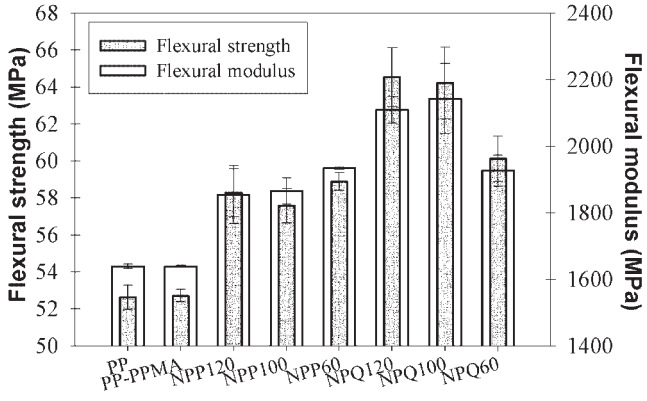

FIG. 13. Flexural properties of the PP, PP-PPMA, and PNC.

pounding condition with proper screw speed and shear stress should also be employed to promote further clay microdispersion and possible exfoliation.

ACKNOWLEDGMENTS

The first author thank the National Science and Engineering Research Council Canada for a fellowship. The authors show appreciation to Dr. Utracki for thoughtful discussions. The authors also thank F. Perrin-Sarazin, W. Leelapornpisit, and M. Plourde for their technical work.

REFERENCES

1. A. Usuki, Y. Kojima, M. Kawasumi, A. Okada, T. Kurauchi, and O. Kamigaito, *J. Mater. Res.*, **5**, 8 (1993).
2. L.A. Utracki, *Clay-Containing Polymeric Nanocomposites*, RAPRA, Shawsburg, Shropshire, UK (2004).
3. K. Yano, A. Usuki, A. Okada, T. Kurauchi, and O. Kamigaito, *J. Polym. Sci. Part A: Polym. Chem.*, **31**, 2493 (1993).
4. R. Krishnamoorti, R. Vaia, and E. Giannelis, *Chem. Mater.*, **8**, 1728 (1996).
5. G. Jimenez, N. Ogata, H. Kawai, and T. Ogihara, *J. Appl. Polym. Sci.*, **64**, 2211 (1997).
6. A. Weiss, *Clays Clay Miner.*, **10**, 191 (1963).
7. A. Okada, A. Usuki, T. Kurauchi, and O. Kamigaito, *ACS Symp. Ser.*, **585**, 55 (1995).
8. P. Messersmith and E. Giannelis, *J. Polym. Sci. Part A: Polym. Chem.*, **33**, 1047 (1995).
9. A. Akelah and A. Moet, *J. Mater. Sci.*, **31**, 3589 (1996).
10. T. Von Werne and T. Patten, *J. Am. Chem. Soc.*, **121**, 7409 (1999).
11. P. Reichert, B. Hoffmann, T. Bock, R. Thomann, and R. Mülhaupt, *Macromol. Rapid Commun.*, **22**, 519 (2001).
12. J. Cho and D. Paul, *Polymer*, **42**, 1083 (2001).
13. Y, Wang, F. Chen, and K. Wu, *J. Appl. Polym. Sci.*, **93**, 100 (2004).
14. S. Burnside, H. Chen, and E. Giannelis, *Chem. Mater.*, **7**, 1597 (1995).
15. R. Vaia, K. Jandt, E. Kramer, and E. Giannelis, *Chem. Mater.*, **8**, 2628 (1996).
16. R. Vaia and E. Giannelis, *Macromolecules*, **30**, 8000 (1997).
17. X. Liu and Q. Wu, *Polymer*, **42**, 1001 (2001).
18. Q. Zhang, Q. Fu, L. Jiang, and Y. Lei, *Polym. Int.*, **49**, 1561 (2001).
19. M.-T. Ton-That, F. Perrin-Sarazin, K.C. Cole, M. Bureau, and J. Denault, *Polym. Eng. Sci.*, **44**, 1212 (2004).
20. Y. Wang, F. Chen, Y. Li, and K. Wu, *Compos. B,* **35**, 111 (2004).
21. H. Dennis, D. Hunter, D. Chang, S. Kim, J. White, J. Cho, and D. Paul, *Polymer*, **42**, 9513 (2001).
22. M. Kato, M. Mitsumasa, and K. Fukumori, *Polym. Eng. Sci.*, **44**, 1205 (2004).
23. E. Manias, A. Touny, L. Wu, K. Strawhecker, B. Lu, and T.C. Chung, *Chem. Mater*, **13**, 3516 (2001).
24. L.A. Utracki, M. Sepehr, and J. Li, *Int. Polym. Process.*, accepted (2006).
25. N. Hasegawa, M. Kawasumi, and M. Kato, *J. Appl. Polym. Sci.*, **67**, 67 (1998).
26. (a) M. Kawasumi, M. Hasegawa, and M. Kato, *Macromolecules*, **30**, 6333 (1997); (b) P. Reichert, H. Nitz, S. Klinke, R. Braudsch, R. Thommann, and R. Mülhaupt, *Macromol. Mater. Eng.*, **275**, 8 (2000).
27. A. Oya, Y. Kurokawa, and H. Yasuda, *J. Mater. Sci.*, **35**, 1042 (2000).
28. K. Kim, L.A. Utracki, and M.R. Kamal, *J. Chem. Phys.*, **121**, 10766 (2004).

 DOI 10.1002/pen